High Power Laser Science and Engineering, (2023), Vol. 11, e59, 5 pages.
doi:10.1017/hpl.2023.58

HIGH POWER LASER SCIENCE AND ENGINEERING

RESEARCH ARTICLE

Spatiotemporally mode-locked soliton fiber laser at 2.8 μm

Ying'an Chen, Yicheng Zhou, Zhipeng Qin, Guoqiang Xie, Peng Yuan, Jingui Ma, and Liejia Qian

School of Physics and Astronomy, Key Laboratory for Laser Plasmas (Ministry of Education), Collaborative Innovation Center of IFSA (CICIFSA), Shanghai Jiao Tong University, Shanghai, China

(Received 30 May 2023; revised 24 June 2023; accepted 28 June 2023)

Abstract

Spatiotemporal mode-locking creates great opportunity for pulse energy scaling and nonlinear optics research in fiber. Until now, spatiotemporal mode-locking has only been realized in normal-dispersion dissipative soliton and similariton fiber lasers. In this paper, we demonstrated the first experimental realization of a spatiotemporally mode-locked soliton laser in mid-infrared fluoride fiber with anomalous dispersion. The mode-locked fluoride fiber oscillator directly generated a record pulse energy of 16.1 nJ and peak power of 74.6 kW at 2.8 μm wavelength. This work extends the spatiotemporal mode-locking to soliton fiber lasers and should have a wide interest for the laser community.

Keywords: mid-infrared; soliton fiber laser; spatiotemporal mode-locking

1. Introduction

In recent years, multimode fiber has gained a great deal of attention as a new platform to study complex nonlinear interaction and mode-locking dynamics[1–5]. Some novel phenomena and physics mechanisms, such as self-beam cleaning, mode self-organization, and acceleration of wave condensation, have been found in multimode fiber. In 2017, Wright *et al.* [6] first realized spatiotemporal mode-locking in a multimode fiber laser, in which the longitudinal modes and transverse modes are locked in phase and thus the laser generates a variety of spatiotemporal profiles[7]. The spatiotemporal mode-locking extends 1D longitudinal mode-locking to 3D longitudinal and transverse mode-locking, and provides a platform for complex nonlinear interaction and mode-locking dynamic research. Meanwhile, spatiotemporal mode-locking in multimode fiber expands the effective area of fibers and has the potential to significantly improve the mode-locked pulse energy of fiber lasers. Spatiotemporal mode-locking should be very attractive for the pulse energy scaling of soliton fiber lasers, in which the pulse energy is limited according to the soliton area theorem[8]. So far, spatiotemporal mode-locking has been realized in dissipative soliton, similariton and dispersion-managed soliton fiber lasers and Mamyshev oscillators around the 600 nm, 1 μm and 1.5 μm wavebands[9–16].

In the most recent decade, fluoride fiber mode-locked lasers around 3 μm wavelength have attracted wide interest due to their great potential in mid-infrared supercontinuum generation, molecular spectroscopy, medical surgery, semiconductor processing and frequency down-conversion[17–24]. Since fluoride gain fiber has a large anomalous dispersion, fluoride fiber mode-locked lasers generally operate in the soliton regime[25–30] and the mode-locked pulse energy is limited by the soliton area. Through dispersion management, the pulse energy of mode-locked fluoride fiber lasers has been increased a number of times[31,32]. Due to the anomalous dispersion of fluoride fiber in the mid-infrared region, it is difficult to realize the dissipative soliton and similariton in fluoride fiber, which generally can produce higher pulse energy. Thus, it should be interesting to demonstrate spatiotemporal mode-locking in mid-infrared fluoride fiber, which may significantly scale up the pulse energy by exploiting multimode fiber with a large mode area.

In this paper, we report on a spatiotemporally mode-locked soliton fiber laser for the first time. By using Er^{3+}-doped ZBLAN multimode fiber as the gain medium and nonlinear polarization rotation (NPR) mode-locking, spatiotemporal mode-locking was realized. The spatiotemporally mode-locked soliton fiber oscillator directly produced a record pulse energy of 16.1 nJ and peak power of 74.6 kW, with average output power reaching 1.09 W at 2.8 μm wavelength.

Correspondence to: Guoqiang Xie, School of Physics and Astronomy, Key Laboratory for Laser Plasmas (Ministry of Education), Collaborative Innovation Center of IFSA (CICIFSA), Shanghai Jiao Tong University, Shanghai 200240, China. Email: xiegq@sjtu.edu.cn

The soliton pulse energy has the potential to be further improved by adopting larger-core multimode fiber. This work extends spatiotemporal mode-locking to the soliton regime and mid-infrared wavelength, and should be interesting for the laser community.

2. Experimental setup

The experimental setup of the spatiotemporally mode-locked soliton Er:ZBLAN fiber laser is illustrated in Figure 1. A fiber-coupled laser diode (LD) operating at 976 nm was used as a pump source. The core diameter of the pigtailed fiber is 105 μm, and the numerical aperture (NA) is 0.22. The maximum output power from the LD is 30 W. The pump beam was collimated by a spherical lens L_1 ($f = 10$ mm) and then focused by an aspherical lens L_2 ($f = 12.7$ mm) into an Er^{3+}-doped double cladding ZBLAN fiber (FiberLabs, Japan). The multimode Er:ZBLAN fiber has a core diameter of 30 μm with a length of 2.4 m and an Er-doping concentration of 6%. The refractive indices of the core and clad at 2.8 μm wavelength are 1.4916 and 1.4850, respectively. The NA of the Er:ZBLAN fiber is 0.14. The group velocity dispersion (GVD) of the fiber at 2.8 μm wavelength is –110.5 fs^2/mm. The pump absorption ratio of the fiber is 3–5 dB/m, and the fiber loss at 2.8 μm wavelength is 0.1–0.2 dB/m. The V parameter of the fiber at 2.8 μm wavelength is 4.72, which supports approximately eight transverse modes. The cladding diameter of the Er:ZBLAN fiber was 300 μm for efficiently coupling the pump light into the fiber. The two end facets of the fiber were cleaved at an 8° angle, avoiding parasitic oscillation from the fiber facets. The 2.8 μm laser from the gain fiber was collimated by aspherical lens L_3 with a focal length of 12.7 mm. The utilization of an aspherical lens will reduce the adverse effects caused by the aberrations. The output coupler (OC) had a transmission of 40%. A half-wave plate (HWP), an isolator including polarizers and a quarter-wave plate (QWP) were inserted into the cavity for realizing the mode-locking of NPR[33]. The isolator had a cleaning diameter of 4 mm, which could serve as a spatial filter for spatiotemporal mode-locking. The HWP, isolator and QWP were coated with a high transmission at 2.8 μm wavelength. A 45°-placed dichroic mirror (high reflectivity for 2.8 μm and high transmission for 976 nm) was used to combine the pump beam and laser beam, and then the two beams were coupled into the gain fiber through aspherical lens L_2. The forward-pumping scheme was applied, which helps faster accumulation of nonlinear phase shift for NPR mode-locking.

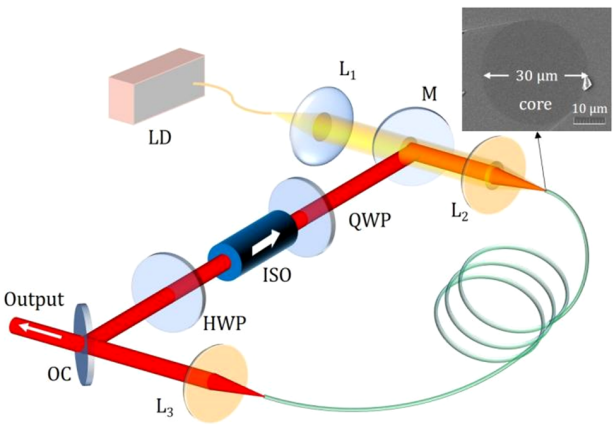

Figure 1. Schematic of the spatiotemporally mode-locked soliton Er:ZBLAN fiber laser. LD, laser diode; L_1, spherical lens; L_2 and L_3, aspherical ZnSe lenses; M, dichroic mirror; OC, output coupler; HWP, half-wave plate; QWP, quarter-wave plate; ISO, isolator. Inset: the enlargement of the fiber facet obtained by a scanning electron microscope, showing a 30-μm fiber core diameter.

The coexistence of multiple transverse modes is of vital importance, as it is the prerequisite for realizing spatiotemporal mode-locking. In the experiment, the axial positions of two aspherical lenses L_2 and L_3 could be adjusted to control the high-order transverse modes. The off-focus of the two aspherical lenses will couple the beam into high-order modes. In addition, the off-focus of the two aspherical lenses also changes the beam size on the isolator, which acts as a spatial filter. In the experiment, the isolator cleaning aperture was only a little larger than the size of the fundamental mode, which helps to filter very high-order transverse modes. The spatial filtering effect of the isolator is helpful to realize stable spatiotemporal mode-locking.

3. Experimental result and discussion

The output beam patterns of the fiber laser were recorded by a mid-infrared charge-coupled device (CCD; Tigris-MWIR-MCTBB-640, Xenics), as shown in Figures 2(a)–2(d). From the beam patterns, we clearly observed the coexisting multiple transverse modes oscillation. The beam profile in continuous-wave (CW) operation (Figure 2(a)) was obviously different from those in spatiotemporal mode-locking operations (Figures 2(b)–2(d)), as observed in a spatiotemporally mode-locked laser[6]. However, in spatiotemporal mode-locking operation, the beams have very similar profiles in spite of different pump powers. In addition, the M^2 factor was also measured with the knife-edge method in the spatiotemporal mode-locking operation, as shown in Figure 2(e). The M^2 factors in the x and y directions were measured to be 2.93 and 2.84, respectively, further showing multiple transverse mode operation in the mode-locked laser.

Through finely adjusting the waveplates, stable spatiotemporal mode-locking could be realized in the multimode fiber laser. A high-speed mid-infrared photoelectric detector and an oscilloscope with 1 GHz bandwidth were used to record the mode-locked pulse trains. The spatiotemporal mode-locking shows stable mode-locking pulse trains at the nanosecond and millisecond scales (Figure 3(a)), with a

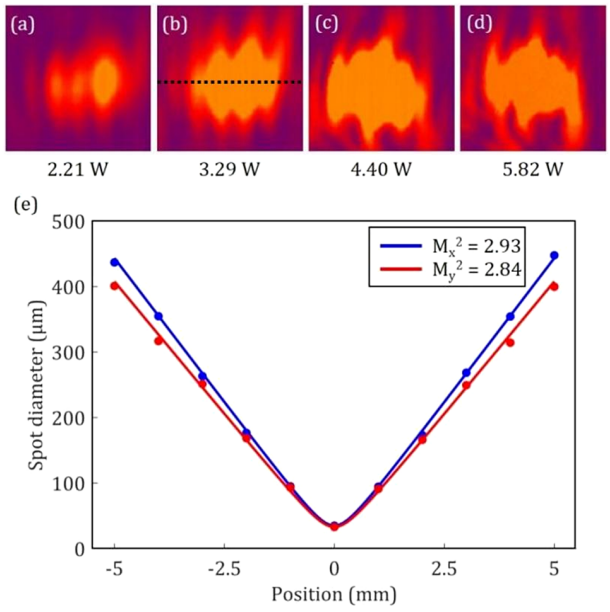

Figure 2. (a) The output beam pattern recorded in continuous-wave operation. (b)–(d) The output beam patterns recorded in spatiotemporal mode-locking operation at different pump powers. (e) The measured M^2 factors of the output beam at pump power of 4.40 W in the spatiotemporal mode-locking operation.

pulse period of approximately 15 ns. To further test the simultaneous mode-locking of multiple transverse modes, we sampled the mode-locked pulse trains at different spatial positions in the beam by placing a pinhole in front of the photoelectric detector. The pinhole and the photoelectric detector can be moved for sampling. The mode-locked pulse trains at different spatial positions along *x*-axis (dashed line in Figure 2(b)) are recorded, as shown in Figure 3(b). For the different positions in the beam of multiple transverse modes, mode-locked pulse trains could be observed. Besides, the intensities of the pulse trains detected at different spatial positions are plotted in Figure 3(c). The intensities show an irregular change without symmetry along the *x*-axis, also suggesting that mode-locking is made up of multiple transverse modes, because single-transverse-mode mode-locked pulse intensity should be symmetrical along the *x*-axis. These mean the generation of spatiotemporal mode-locking in the laser.

The radio-frequency (RF) spectrum in Figure 4(a) shows a signal-to-noise ratio (SNR) of 71 dB at the fundamental frequency of 68 MHz. The intensity roll-off in the wide-range RF spectrum was due to the limited bandwidth of the mid-infrared detector. The high SNR indicates that a stable CW mode-locking was realized. The pulse duration of the mode-locked pulses was measured with a commercial mid-infrared autocorrelator. As shown in Figure 4(b), the mode-locked pulses have a pulse duration of 216 fs, assuming a sech^2 pulse profile. The output spectrum of the spatiotemporally mode-locked fiber laser was measured with a mid-infrared spectral analyzer, which covers a wide range of 1–5 μm wavelength. The central wavelength of the mode-locked pulse was located at 2.8 μm, as shown in Figure 4(c). From the mode-locking spectrum, a Kelly sideband can be observed, which is a typical characteristic of soliton mode-locking. The sidebands of shorter wavelength disappear, which may be attributed to vapor absorption in this band.

In the experiment, the minimum pump power that initiated soliton mode-locking was 3.29 W, and the corresponding average output power was 335 mW. As we increased the pump power, the average output power increased linearly

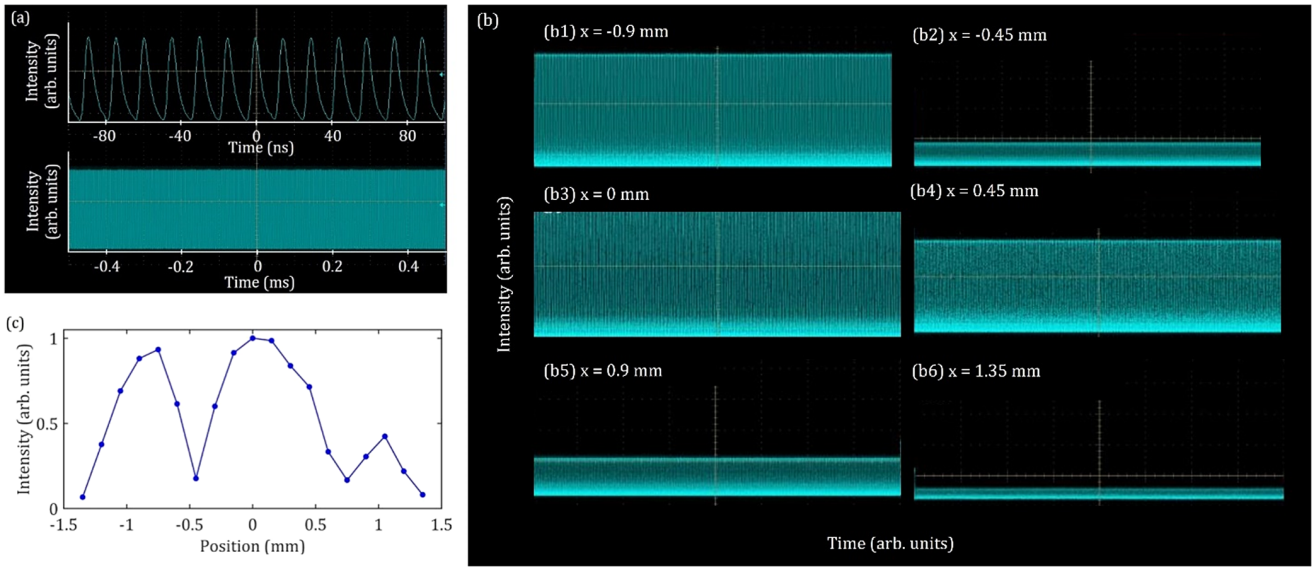

Figure 3. (a) Recorded mode-locked pulse trains in the 200 ns and 1 ms time scales. (b) Sampled pulse trains at different spatial positions. (c) Intensities of sampled pulse trains versus spatial positions.

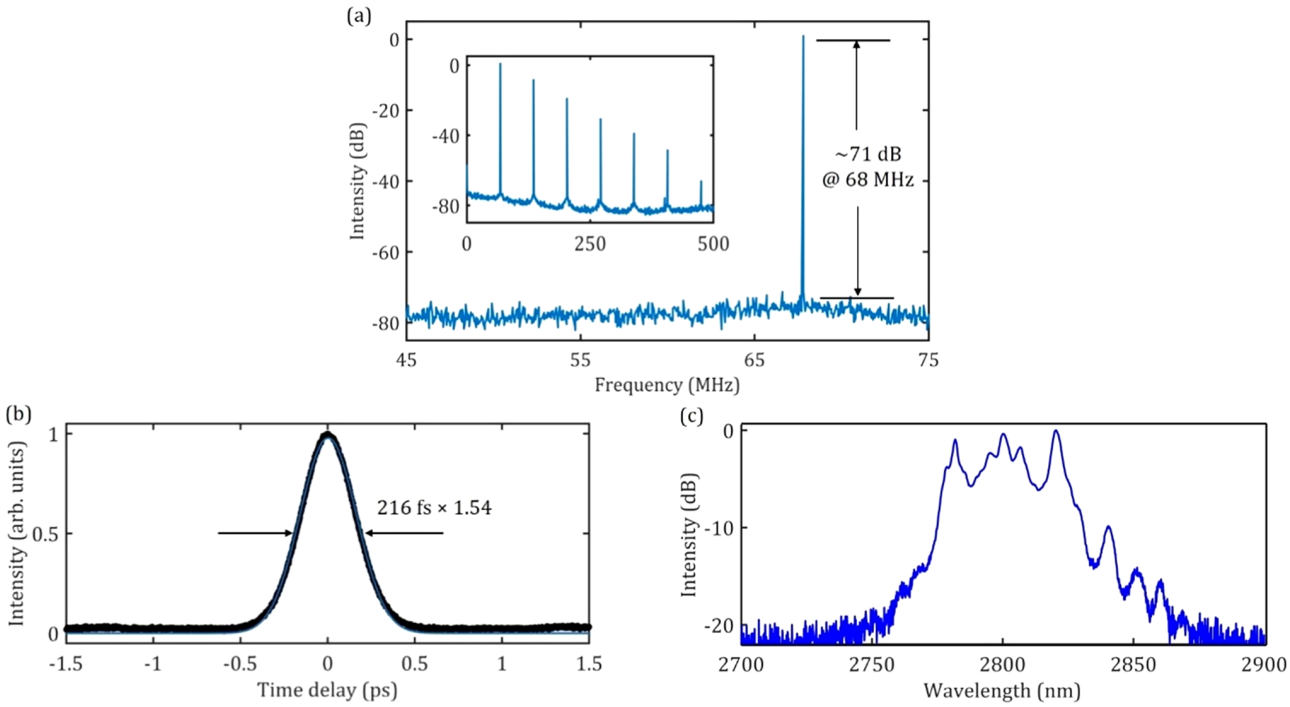

Figure 4. (a) Measured radio-frequency (RF) spectrum of the mode-locked pulses. Inset: RF spectrum with 500 MHz span. (b) Measured autocorrelation trace of the mode-locked pulses (black dots) with a sech^2 fit (blue solid line). (c) Optical spectrum of mode-locked pulses. These results were measured under the average output power of 1.09 W.

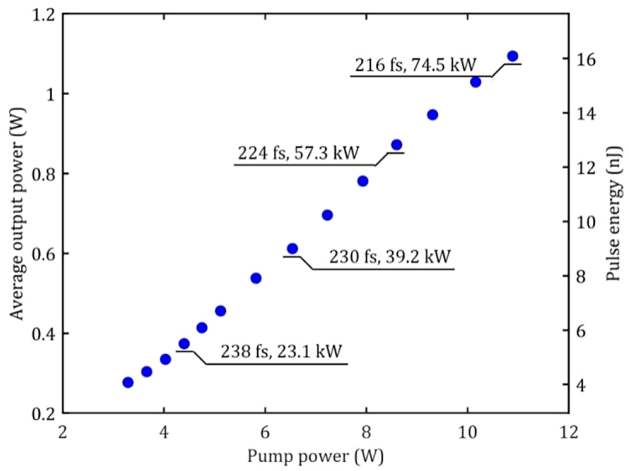

Figure 5. The output average power and pulse energy versus pump power for the spatiotemporally mode-locked soliton fiber laser. The recorded data are the corresponding pulse duration and peak power.

with a slope efficiency of 10.4%, as shown in Figure 5. The pulse duration slightly decreased with the increase of the pump power, which is due to the spectrum broadening induced by self-phase modulation. The achieved maximum average output power was 1.09 W under the pump power of 10.89 W. Considering the pulse duration of 216 fs and the repetition rate of 68 MHz, the corresponding pulse energy and peak power were 16.1 nJ and 74.5 kW, respectively.

Soliton splitting and collapse will occur in a soliton laser if excessive nonlinear phase shift is accumulated. Soliton splitting was observed in the mode-locked soliton fluoride fiber laser when the pulse energy reached 7.6 nJ[27]. In our work, soliton splitting and collapse were not observed even though a much higher pulse energy was generated. This is due to the extension of the spatial scale resulting from spatiotemporal mode-locking. According to the soliton area theorem, the soliton area is inversely proportional to the nonlinear parameter γ, and the nonlinear parameter γ is inversely proportional to the guiding mode area of the fiber. Therefore, the larger guiding mode area of multimode fiber decreases the nonlinear parameter γ, and thus increases the upper limit of soliton pulse energy.

The pulse energy of the soliton Er:ZBLAN fiber laser has potential to be further improved. For example, using a commercially available Er^{3+}-doped ZBLAN fiber with a 70-μm core diameter, the guiding mode area will be enlarged by more than 20 times compared to a single mode fiber. The spatiotemporally mode-locked soliton pulse energy is expected to exceed 100 nJ, and the pulse peak power is expected to reach hundreds of kilowatts. This means that it is possible to scale up the soliton pulse energy and peak power in the mid-infrared region by an order of magnitude, promising a wide application prospect.

The pulse energy from fiber mode-locked lasers has exceeded the microjoule level around the 1 μm wavelength[34]. However, the pulse energy of 3 μm mode-locked

fiber lasers was lower by two orders of magnitude since the existing high-energy mode-locking pulse mechanisms, such as the dissipative soliton and similariton, are difficult to operate in anomalous-dispersion fibers. So far, pulse energies from 3 μm femtosecond mode-locked fiber lasers have not exceeded 10 nJ yet, even though various methods have been tried[27–32]. The introduction of spatiotemporal mode-locking to the mid-infrared region creates the possibility for narrowing the gap with the near-infrared region.

4. Conclusion

In conclusion, we successfully demonstrated a spatiotemporally mode-locked soliton fiber laser for the first time. By using Er:ZBLAN fiber with anomalous dispersion as the gain medium and NPR mode-locking, soliton spatiotemporal mode-locking was realized with an SNR of 71 dB. Using Er:ZBLAN fiber with a core diameter of 30 μm, the spatiotemporally mode-locked soliton fiber laser directly produced a record pulse energy of 16.1 nJ and peak power of 74.5 kW at 2.8 μm wavelength; the corresponding average output power reached 1.09 W with pulse duration of 216 fs. The mid-infrared pulse energy and peak power have potential to be further scaled up if the spatial scale of the fiber is further enlarged. The work provides a feasible way to scale up the pulse energy and peak power of mid-infrared mode-locked fiber lasers.

Acknowledgements

This work was partially supported by the National Natural Science Foundation of China (Nos. 62075126 and 62005161) and the Fundamental Research Funds for the Central Universities.

References

1. L. G. Wright, W. H. Renninger, D. N. Christodoulides, and F. W. Wise, Opt. Express **23**, 3492 (2015).
2. L. G. Wright, Z. Liu, D. A. Nolan, M. J. Li, D. N. Christodoulides, and F. W. Wise, Nat. Photonics **10**, 771 (2016).
3. L. G. Wright, D. N. Christodoulides, and F. W. Wise, Nat. Photonics **9**, 306 (2015).
4. K. Krupa, A. Tonello, B. M. Shalaby, M. Fabert, A. Barthelemy, G. Millot, S. Wabnitz, and V. Couderc, Nat. Photonics **11**, 237 (2017).
5. A. Fusaro, J. Garnier, K. Krupa, G. Millot, and A. Picozzi, Phys. Rev. Lett. **122**, 123902 (2019).
6. L. G. Wright, D. N. Christodoulides, and F. W. Wise, Science **358**, 94 (2017).
7. L. G. Wright, P. Sidorenko, H. Pourbeyram, Z. M. Ziegler, A. Isichenko, B. A. Malomed, C. R. Menyuk, D. N. Christodoulides, and F. W. Wise, Nat. Phys. **16**, 565 (2020).
8. A. Hasegawa and F. Tappert, Appl. Phys. Lett. **23**, 142 (1973).
9. T. Mayteevarunyoo, B. A. Malomed, and D. V. Skryabin, Opt. Express **27**, 37364 (2019).
10. H. Qin, X. Xiao, P. Wang, and C. Yang, Opt. Lett. **43**, 1982 (2018).
11. Y. Ding, X. Xiao, P. Wang, and C. Yang, Opt. Express **27**, 11435 (2019).
12. U. Tegin, E. Kakkava, B. Rahmani, D. Psaltis, and C. Moser, Optica **6**, 1412 (2019).
13. U. Tegin, E. Kakkava, B. Rahmani, D. Psaltis, and C. Moser, in *Conference on Lasers and Electro-Optics (CLEO)* (2020), paper SM4P.1.
14. H. Haig, P. Sidorenko, A. Dhar, N. Choudhury, R. Sen, D. N. Christodoulides, and F. W. Wise, Opt. Lett. **47**, 46 (2022).
15. Y. Wu, D. N. Christodoulides, and F. W. Wise. Opt. Lett. **47**, 4439 (2022).
16. B. Cao, C. Gao, Y. Ding, X. Xiao, C. Yang, and C. Bao. Opt. Lett. **47**, 4584 (2022).
17. C. Wei, X. Zhu, R. A. Norwood, and N. Peyghambarian, Opt. Lett. **37**, 3849 (2012).
18. Z. Qin, G. Xie, C. Zhao, S. Wen, P. Yuan, and L. Qian, Opt. Lett. **41**, 56 (2016).
19. Z. Qin, T. Hai, G. Xie, J. Ma, P. Yuan, L. Qian, L. Li, L. Zhao, and D. Shen, Opt. Express **26**, 8224 (2018).
20. J. Ma, Z. Qin, G. Xie, L. Qian, and D. Tang, Appl. Phys. Rev. **6**, 021317 (2019).
21. C. R. Petersen, U. Møller, I. Kubat, B. Zhou, S. Dupont, J. Ramsay, T. Benson, S. Sujecki, N. Abdel-Moneim, Z. Tang, D. Furniss, A. Seddon, and O. Bang, Nat. Photonics **8**, 830 (2014).
22. F. Tittel, D. Richter, and A. Fried, in *Solid-State Mid-Infrared Laser Sources*, Topics in Applied Physics (Springer, 2003), p. 458.
23. S. Amini-Nik, D. Kraemer, M. L. Cowan, K. Gunaratne, P. Nadesan, B. A. Alman, and R. J. D. Miller, PLoS ONE **5**, e13053 (2010).
24. A. H. Nejadmalayeri, P. R. Herman, J. Burghoff, M. Will, S. Nolte, and A. Tünnermann, Opt. Lett. **30**, 964 (2005).
25. S. Duval, M. Bernier, V. Fortin, J. Genest, M. Piche, and R. Vallee, Optica **2**, 623 (2015).
26. T. Hu, S. D. Jackson, and D. D. Hudson, Opt. Lett. **40**, 4226 (2015).
27. S. Antipov, D. D. Hudson, A. Fuerbach, and S. D. Jackson, Optica **3**, 1373 (2016).
28. H. Gu, Z. Qin, G. Xie, T. Hai, P. Yuan, J. Ma, and L. Qian, Chin. Opt. Lett. **18**, 031402 (2020).
29. L. Yu, J. Liang, S. Huang, J. Z. Wang, J. C. Wang, X. Luo, P. Yan, F. Dong, X. Liu, Q. Lue, C. Guo, and S. Ruan, Photonics Res. **10**, 2140 (2022).
30. L. Yu, J. Liang, S. Huang, J. Wang, J. Wang, X. Luo, P. Yan, F. Dong, X. Liu, Q. Lue, C. Guo, and S. Ruan, Opt. Lett. **47**, 2562 (2022).
31. Z. Qin, G. Xie, H. Gu, T. Hai, P. Yuan, J. Ma, and L. Qian, Adv. Photonics **1**, 065001 (2019).
32. J. Huang, M. Pang, X. Jiang, F. Köttig, D. Schade, W. He, M. Butryn, and P. St. J. Russell, Optica **7**, 574 (2020).
33. M. Hofer, M. E. Fermann, F. Haberl, M. H. Ober, and A. J. Schmidt, Opt. Lett. **16**, 502 (1991).
34. W. Liu, R. Liao, J. Zhao, J. Cui, Y. Song, C. Wang, and M. Hu, Optica **6**, 194 (2019).